Thermosensitive TRPV Channel Subunits Coassemble into Heteromeric Channels with Intermediate Conductance and Gating Properties

Wei Cheng, Fan Yang, Christina L. Takanishi, and Jie Zheng

Department of Physiology and Membrane Biology, University of California, Davis, School of Medicine, Davis, CA 95616

Heat-sensitive transient receptor potential (TRP) channels (TRPV1–4) form the major cellular sensors for detecting temperature increases. Homomeric channels formed by thermosensitive TRPV subunits exhibit distinct temperature thresholds. While these subunits do share significant sequence similarity, whether they can coassemble into heteromeric channels has been controversial. In the present study we investigated the coassembly of TRPV subunits using both spectroscopy-based fluorescence resonance energy transfer (FRET) and single-channel recordings. Fluorescent protein–tagged TRPV subunits were coexpressed in HEK 293 cells; FRET between different subunits was measured as an indication of the formation of heteromeric channels. We observed strong FRET when fluorescence signals were collected selectively from the plasma membrane using a "spectra FRET" approach but much weaker or no FRET from intracellular fluorescence. In addition, no FRET was detected when TRPV subunits were coexpressed with members of the TRPM subfamily or CLC-0 chloride channel subunits. These results indicate that a substantial fraction of TRP channels in the plasma membrane of cotransfected cells were heteromeric. Single-channel recordings confirmed the existence of multiple heteromeric channel forms. Interestingly, heteromeric TRPV channels exhibit intermediate conductance levels and gating kinetic properties. As these subunits coexpress both in sensory neurons and in other tissues, including heart and brain, coassembly between TRPV subunits may contribute to greater functional diversity.

The Journal of General Physiology

INTRODUCTION

Transient receptor potential (TRP) channels form a group of cation channels that serve as cellular sensors for various physical and chemical stimuli (Clapham et al., 2001; Minke and Cook, 2002; Montell et al., 2002; Clapham, 2003). Based on sequence similarities, mammalian TRP channels are divided into six subfamilies including the canonical or classical TRPs (TRPC), the osm-9–like or vanilloid receptor TRPs (TRPV), the melastatin or long TRPs (TRPM), the mucolipins (TRPML), the polycystins (TRPP), and ankyrin transmembrane protein 1 (TRPA1) (Clapham et al., 2003). Within the TRPV subfamily there is a unique group of four channels, TRPV1, TRPV2, TRPV3, and TRPV4, that recently have been identified as the major cellular sensors for detecting increases in temperature (Jordt et al., 2003; Patapoutian et al., 2003; Voets et al., 2005; Dhaka et al., 2006). When expressed in heterologous expression systems, these thermosensitive channels convey temperature sensitivity to the host cells, suggesting that the channel protein is sufficient to convert changes in thermal energy into electrical activity. The temperature thresholds for thermosensitive TRPV channels are graded, with TRPV4 being activated by innocuous warm temperatures (>27°C) (Guler et al., 2002; Watanabe et al., 2002; Chung et al., 2003), TRPV3 by higher temperatures (between 31°C and 39°C) (Peier et al., 2002; Smith et al., 2002; Xu et al., 2002), TRPV1 by hot temperatures (>43°C) (Caterina et al., 1997; Caterina et al., 2000), and TRPV2 by noxious temperatures (>52°C) (Caterina et al., 1999; Ahluwalia et al., 2002). Collectively, these channels cover a broad range of ambient temperatures that humans can distinguish.

TRP channels are members of the tetrameric cation channel superfamily (Jahnel et al., 2001; Kedei et al., 2001; Kuzhikandathil et al., 2001), for which subunit composition is a major determinant of the biophysical and regulatory properties of each channel type (Hille, 2001). Heteromeric channel formation has been widely reported for TRP channels within the TRPC and TRPM subfamilies (Xu et al., 1997; Lintschinger et al., 2000; Strubing et al., 2001; Goel et al., 2002; Hofmann et al., 2002; Amiri et al., 2003; Strubing et al., 2003; Chubanov et al., 2004; Liu et al., 2005; Li et al., 2006; Poteser et al., 2006). However, whether TRPV subunits can coassemble into heteromeric channels has been the subject of debate (Schaefer, 2005). For example, when TRPV3 was originally cloned it was found to coassemble with TRPV1 to form heteromeric channels with altered pharmacological properties (Smith et al., 2002). However, a later study rejected

Correspondence to Jie Zheng: JZheng@ucdavis.edu

Abbreviations used in this paper: eYFP, enhanced yellow fluorescent protein; FRET, fluorescence resonance energy transfer; HEK, human embryonic kidney; HMM, hidden Markov modeling; TRP, transient receptor potential.

the existence of coassembly between TRPV1 and TRPV3, based on results from colocalization, coimmunoprecipitation, and fluorescence resonance energy transfer (FRET) experiments (Hellwig et al., 2005). This later study further suggested that when coexpressed in cultured cells, all four thermosensitive TRPV subunits preferentially assemble into homomeric channels, despite the high sequence similarity shared by these subunits.

Whether thermosensitive TRPV channels coassemble into heteromeric channels has important implications for the coding and regulation of thermosensation. For this reason, we investigated TRPV coassembly in detail in live cells using a combination of FRET and single-channel recordings. Like the previous study by Hellwig et al. (2005), we assessed coassembly of TRPV subunits with a FRET technique in human embryonic kidney (HEK) cells cotransfected with pairs of TRPV subunits that were labeled with GFP mutants (Tsien, 1998). FRET is a process in which the light energy absorbed by a donor fluorophore is transferred to a nearby acceptor fluorophore through electromagnetic field interaction (Clegg, 1992; Selvin, 1995). The efficiency of energy transfer falls off exponentially to the sixth power of the distance between the fluorophores; it drops to practically zero for GFP mutant–based FRET pairs when they are >10 nm apart. This makes FRET a particularly powerful technique to monitor subunit interactions in multisubunit proteins like the TRPV channels; positive FRET signals are expected only when the donor- and the acceptor-tagged subunits coassemble into heteromeric channels (Fig. 1). Unlike the study by Hellwig et al. (2005), we limited FRET measurements specifically to the plasma membrane where mature, properly assembled channels are predominantly found. Plasma membrane–specific FRET signals were measured using a spectroscopy-based FRET technique that we refer to as "spectra FRET" (Bykova et al., 2006; Takanishi et al., 2006; Zheng, 2006). In this approach, the spectral and positional information are well preserved, thus allowing reliable quantification of FRET efficiency specifically from the cell membrane. As negative controls, we also measured FRET from the intracellular fluorescence as well as from cells coexpressing TRPV subunits with either members of the TRPM channels subfamily (TRPM4 or TRPM5) or CLC-0 chloride channel subunits. We confirmed our FRET results by electrophysiological experiments in which individual channels from coexpressed cells were recorded. Single-channel properties of individual channels were analyzed and compared with those of the homomeric channels. Results from these experiments suggested that heteromeric TRPV channels are formed by thermosensitive TRPV subunits. These heteromeric channels exhibit unique conductance and gating properties, which may contribute to greater function diversity of thermosensitive channels.

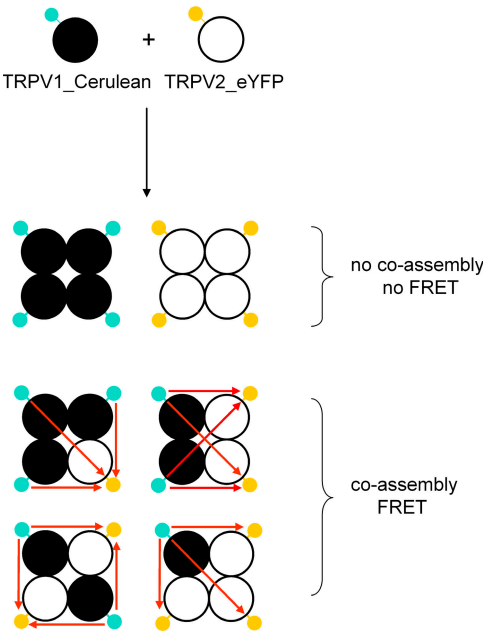

Figure 1. Schematic diagram illustrating the strategy for the FRET experiment. Large circles represent TRPV channel sub units. Small cyan and yellow circles represent Cerulean and eYFP, respectively. Red arrows indicate FRET pathways.

MATERIALS AND METHODS

Constructs

All TRPV constructs used in the present study were based on murine TRPV clones. For FRET recordings, the fluorescence donor was Cerulean, which is a brighter version of the enhanced cyan fluorescent protein (eCFP) due to improved quantum yield (Rizzo et al., 2004); Cerulean also carries a mutation that eliminated the tendency of eCFP to form dimers. The fluorescence acceptor was the enhanced yellow fluorescent protein (eYFP) (Heim and Tsien, 1996). In this report Cerulean and eYFP are referred to as CFP and YFP, respectively. The fluorophore was attached to the C terminus of each channel subunit. All constructs were confirmed by sequencing. Consistent with previous reports on similar constructs (Hellwig et al., 2005), functional recordings of cells transfected with these cDNA constructs did not show noticeable alteration in channel properties from untagged channels. Cell surface expression of each fusion protein was further supported by fluorescence microscopy and patch-clamp recordings.

As negative controls, we coexpressed TRPV constructs with unrelated membrane proteins, including TRPM4_Cerulean, TRPM5_Cerulean, TRPM5_eYFP (gifts from E. Liman, University of Southern California, Los Angeles, CA), and CLC-0_Cerulean (a gift from T.Y. Chen, University of California, Davis, CA). As in TRPV fusion constructs, Cerulean was attached to the C terminus of CLC-0 subunits in CLC-0_Cerulean. For TRPM4 and TRPM5 fusion constructs, the fluorophore was attached to the N terminus. Normal channel functions have been confirmed by the providers of each construct. Surface expression of each protein was confirmed by fluorescence microscopy and electrophysiology.

Cell Transfection

Transfection of HEK 293 cells with cDNA constructs followed standard protocols. In brief, cells were plated at low densities in chambers with a cover-glass bottom (Nunc) and allowed to grow

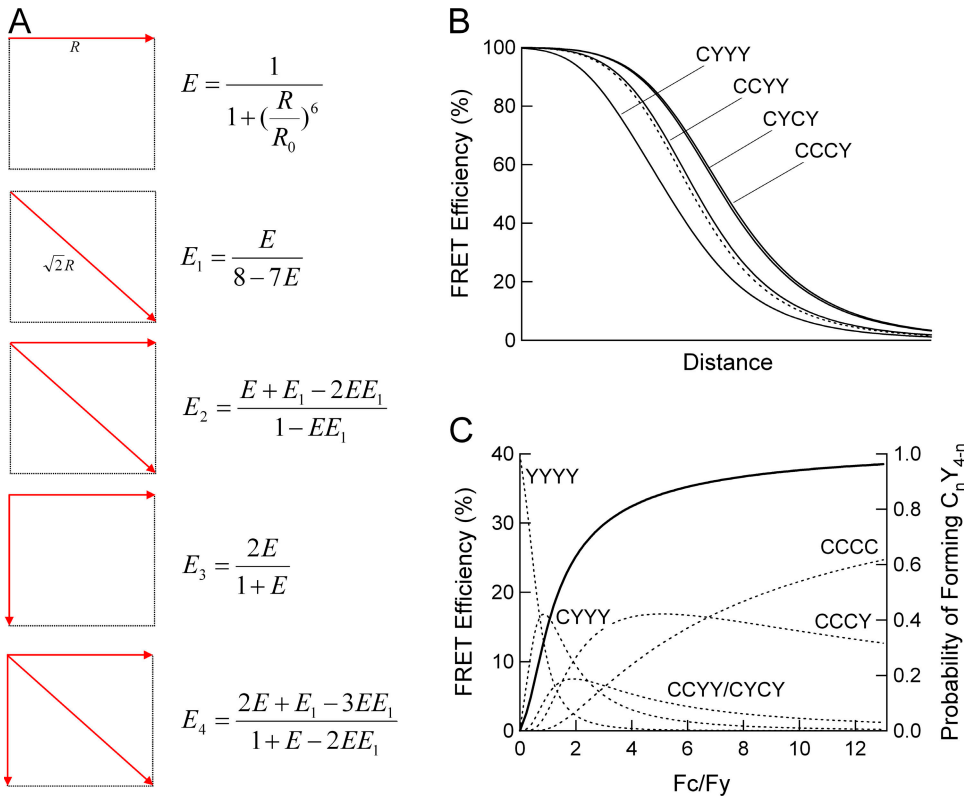

Figure 2. The FRET model. (A) The expected efficiency of energy coupling through various possible pathways within a fourfold symmetric complex. (B) FRET efficiency of each channel type with different subunit stoichiometry (solid curves). For comparison, the FRET efficiency of a single donor–acceptor pair is shown in dotted curve. C, Cerulean; Y, eYFP. (C) The relationship between the fluorescence intensity ratio and the distribution of each channel type (dotted curves) as well as the overall FRET efficiency from all channel populations (solid curve). The value for E is set at 25% for this simulation. Notice that the FRET efficiency curve exhibits significant sigmoidicity and reaches a plateau level much higher than 25%.

overnight in the Dulbecco's modified eagle medium (DMEM) supplemented with 20 mM L-glutamine and 10% FBS. Cells were then transfected with 0.8 µg total cDNA using Lipofectamine 2000 (GIBCO BRL) according to the procedure recommended by the manufacturer. Fluorescence imaging was done at room temperature (22–23°C) 1–2 d after transfection. Right before fluorescence recording, the culture media was replaced with a solution containing (in mM) 130 NaCl, 5 $MgCl_2$, 2 $CaCl_2$, 5 HEPES, and 1 EGTA (pH 7.4).

Electrophysiology

To record single-channel currents from homomeric channels, we transiently transfected HEK 293 cells with TRPV1_Cerulean or TRPV3_Cerulean. For heteromeric channels, we examined cells cotransfected with TRPV1_Cerulean and TRPV3_eYFP. Channel-expressing cells were selected by the presence of Cerulean fluorescence using a 405-nm laser as the excitation light source. Single-channel currents were recorded at room temperature using EPC10 amplifier (HEKA) driven by the PatchMaster software (HEKA). We used the cell-attached configuration to prevent channel rundown. Membrane potential was held at −80 mV from which a voltage step to various levels was used to activate the channel. The bath solution contained (in mM) 150 KCl, 5 $MgCl_2$, 10 HEPES, and 10 glucose (pH 7.4). The pipette solution contained (in mM) 150 NaCl, 1 $MgCl_2$, and 10 HEPES (pH 7.4). Current signals were filtered at 2.9 kHz, and data were sampled at 13.3 kHz. Current amplitude was estimated from all-point histograms constructed with single-channel records digitally filtered at 0.5 kHz. Lifetimes in the open and closed states were estimated with a hidden Markov modeling (HMM) approach (Qin et al., 2000; Zheng et al., 2001; Venkataramanan and Sigworth, 2002) using the QuB software package (http://www.qub.buffalo.edu/); no digital filter was used for these analyses. As the kinetic analysis was mainly used to obtain estimates of the burst duration, the dead-time was set at 0.32 ms to eliminate most of the brief closure events. The distribution of heteromeric channel types was fitted with a binomial distribution, as previously described (Zheng and Sigworth, 1998).

Spectroscopic Microscopy

Epifluorescence microscopy was performed with a fully automated, inverted fluorescence microscope (Olympus IX-81). The excitation light was generated by a 100-mW mercury lamp. The light intensity was controlled by a series of neutral density filters installed in a filter wheel. The duration of light exposure was controlled by a computer-driven mechanical shutter (Olympus IX2-SHA). We used a 60× oil-immersion objective (NA 1.42) in these experiments. Fluorescence emission was detected with a Hamamatsu HQ CCD camera or, in some cases, a Roper 128B CCD camera. For cell imaging, the following filter cubes (Chroma) were used (excitation, dichroic, emission): the CFP cube, D436/20, 455dclp, D480/40; the YFP cube, HQ500/20, Q515lp, HQ535/30. For spectroscopic imaging, a spectrograph (Acton SpectraPro 2150i) was used in conjunction with the camera. In this recording mode two filter cubes (Chroma) were used to collect spectroscopic images from each cell (excitation, dichroic): cube I, D436/20, 455dclp; cube II, HQ500/20, Q515lp. No emission filter was used in these cubes. Under our experimental conditions, autofluorescence from untransfected cells was negligible.

Fluorescence imaging and analysis were done using the MetaMorph software (Universal Imaging). User-designed macros were used for automatic collection of the bright field cell image, the fluorescence cell image, and the spectroscopic image. Emission spectra were collected from the plasma membrane of the cell by positioning the spectrograph slit across a cell and recording the fluorescence intensity at the position corresponding to the membrane region; the same slit position applied to both the spectrum taken with the CFP excitation and the spectrum taken with the YFP excitation. Using this approach, the spectral and positional

TABLE I

FRET Model Parameters

Stoichiometry (C_nY_{4-n})	Probability of forming C_nY_{4-n} ($P_{C_nY_{4-n}}$)	Effective FRET efficiency ($E^C_{C_nY_{4-n}}$)	($E^Y_{C_nY_{4-n}}$)
CCCC	$\frac{r^4}{(1+r)^4}$	0	0
CCCY	$\frac{4r^3}{(1+r)^4}$	$\frac{2E+E_1}{3}$	E_4
CCYY	$\frac{3r^2}{(1+r)^4}$	E_2	E_2
CYCY	$\frac{3r^2}{(1+r)^4}$	E_3	E_3
CYYY	$\frac{4r}{(1+r)^4}$	E_4	$\frac{2E+E_1}{3}$
YYYY	$\frac{1}{(1+r)^4}$	0	0

C represents a Cerulean-containing subunit; Y represents an eYFP-containing subunit; *n*, number of Cerulean-containing subunits; *r*, concentration ratio between C and Y. $E^C_{C_nY_{4-n}}$ and $E^Y_{C_nY_{4-n}}$, effective FRET efficiencies determined by either the decrease in Cerulean emission or the increase in eYFP emission, respectively.

information are well preserved, thus allowing reliable quantification of FRET efficiency specifically from the cell membrane. Spectra were corrected for background light, which was estimated from the blank region of the same image.

Plasma membrane was labeled with di-8-ANEPPS immediately before cell imaging. After the culture media was replaced, 4 μl of 2 mM di-8-ANEPPS (in DMSO) was added to the culture chamber to stain the cell membrane for 10 min in the dark. Free dye was washed away before imaging. Di-8-ANEPPS fluorescence was observed with a filter cube containing (excitation, dichroic, emission) HQ500/20, Q515lp, HQ535/30.

Calculation of FRET Efficiency

For each cell transfected with a pair of channel subunits labeled with either Cerulean or eYFP, two spectroscopic images were taken, one with the Cerulean excitation at 436 nm using cube I, another with the eYFP excitation at 500 nm using cube II. From these two images, the total emission spectrum and the YFP emission spectrum, respectively, were constructed. Standard emission spectra were also collected from cells expressing only Cerulean-tagged subunits or cells expressing only eYFP-tagged subunits. These standard spectra were used to separate the cross-talk contamination between Cerulean and eYFP due to spectra overlaps (Takanishi et al., 2006). The FRET efficiency was calculated from the increase in eYFP emission due to energy transfer using an approach as previously described (Zheng et al., 2002).

Modeling

To apply FRET analysis to TRPV channels, two specific issues must be addressed. (1) As TRPV channels are tetramers (Jahnel et al., 2001; Kedei et al., 2001; Kuzhikandathil et al., 2001), the subunit assembly will bring multiple fluorophores within the FRET distance. The observed FRET efficiency will differ from that of a single donor-to-acceptor pair (Fig. 2). (2) cDNA transfection in culture cells is known to yield highly variable amounts of protein products in individual cells. Accordingly, when Cerulean- and eYFP-tagged subunits are cotransfected, the ratio between the two types of subunits is also highly variable (Bykova et al., 2006; Takanishi et al., 2006). As a result, the measured FRET efficiency is expected to vary from cell to cell. We addressed these issues by developing a mathematical model that describes the dependence of FRET to the channel subunit stoichiometry. The model is based on the following specific assumptions.

(1) We assumed that Cerulean- and eYFP-tagged subunits in the plasma membrane existed only in tetramers.

(2) We further assumed that Cerulean- and eYFP-tagged subunits coassembled randomly into all possible combinations. As a result, the relative concentration of each tetrameric form can be determined by the concentration ratio between Cerulean- and eYFP-tagged subunits, *r*, as defined by the binomial distribution (Table I). For the purpose of the present study, assumptions 1 and 2 are rather safe and conservative, as monomeric subunits or any preferable homomeric assembly, if existed, would cause an underestimate of the FRET efficiency.

(3) To minimize the number of free parameters in the model, all channels were simplified as being fourfold symmetric, even though TRPV subunits may have different structures.

(4) For tetrameric channels containing four fluorophores within FRET distances, there are multiple FRET pathways, as illustrated in Fig. 2. Based on the rate theory for resonance energy transfer (Lakowicz, 1999), the efficiency value associated with each pathway can be calculated from *E*, the FRET efficiency between a donor and an acceptor attached to the neighboring subunits. These efficiency values are shown in Fig. 2 A. To apply these values to tetrameric channels, we further assumed that FRET couplings between these pathways were independent and additive. This last assumption is valid only under low-excitation light conditions, when the fraction of time that a fluorophore spends in the excited state is low. We found that under our experimental conditions, doubling the excitation light intensity nearly doubled the fluorescence emission intensity, suggesting that the fluorescence emission was far from being saturated. Based on the independence assumption, the effective FRET efficiency can be determined for each heteromeric channel types, as shown in Fig. 2 B and Table I.

Under the conditions discussed above, the overall FRET efficiency measured from a cell, E^{app}, and the fluorescence intensity ratio between Cerulean and eYFP, F_C/F_Y, can be calculated according to standard FRET definitions (Selvin, 1995; Takanishi et al., 2006); here FRET is determined as the enhanced emission of the acceptor (eYFP) upon energy transfer. The overall FRET efficiency measured from a cell is

$$E^{app} = \frac{\sum_{n=0}^{4}(4-n)P_{C_nY_{4-n}}E^Y_{C_nY_{4-n}}}{\sum_{n=0}^{4}(4-n)P_{C_nY_{4-n}}}. \quad (1)$$

The fluorescence intensity ration is calculated as

$$\frac{F_C}{F_Y} = \frac{\sum_{n=0}^{4} nP_{C_nY_{4-n}}(1-E^C_{C_nY_{4-n}})}{\sum_{n=0}^{4}(4-n)P_{C_nY_{4-n}}(1+E^Y_{C_nY_{4-n}}\frac{\varepsilon_C}{\varepsilon_Y})}\frac{S_C}{S_Y}. \quad (2)$$

In Eqs. 1 and 2, C_nY_{4-n} represents a channel having *n* Cerulean-containing subunits and $(4-n)$ eYFP-containing subunits ($n = 0$–4), $\varepsilon_C/\varepsilon_Y$ is the molar extinction coefficient ratio between Cerulean and eYFP, and S_C/S_Y is a constant. Both E^{app} and F_C/F_Y are functions of the FRET efficiency between the neighboring subunits, *E*, as well as the concentration ratio between Cerulean- and eYFP-tagged subunits, *r*. When Eqs. 1 and 2 are combined,

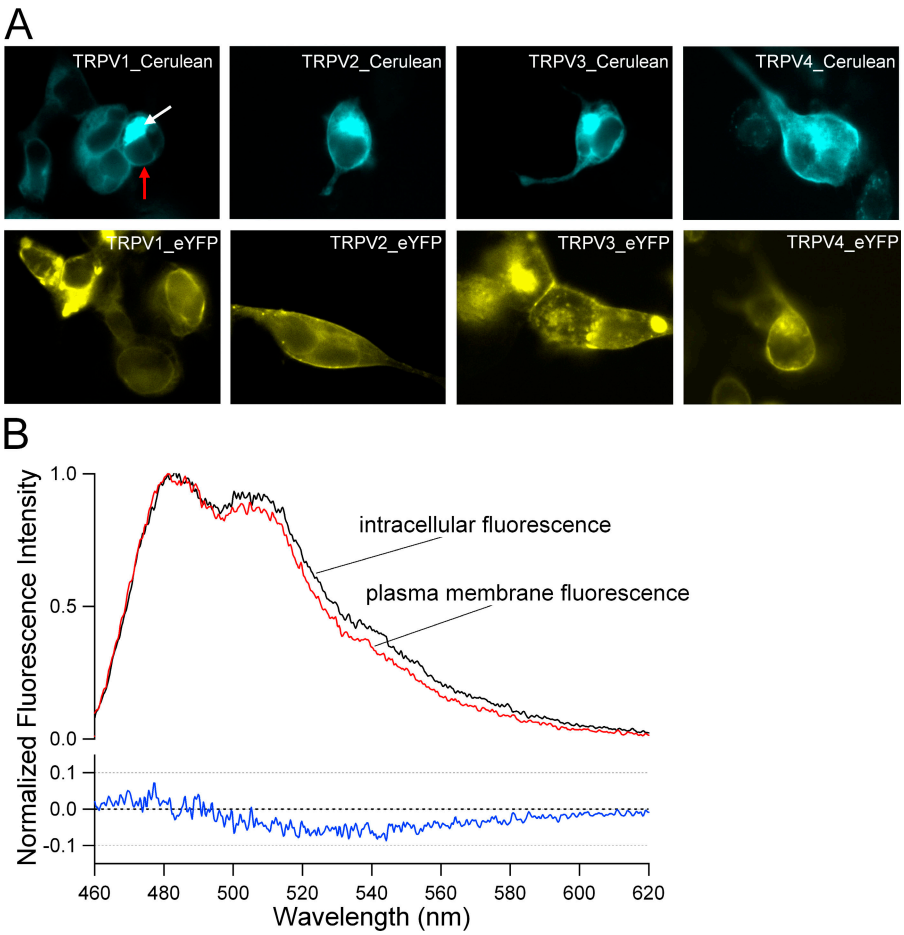

Figure 3. Fluorescence recordings of TRPV expressed in HEK 293 cells. (A) Example cells expressing each of the fluorophore-tagged TRPV subunits. The red and white arrows in the top left panel indicate fluorescence signals from the plasma membrane and the intracellular structures, respectively. (B, top) Emission spectra recorded from the same TRPV1_Cerulean-expressing cell shown in A. (B, bottom) The difference between the plasma and intracellular spectra. Significant difference is observed in the 520–540-nm range, which corresponds to the eYFP peak emission.

the unknown concentration ratio r can be eliminated. This leaves us with two free parameters, the FRET efficiency E and the factor S_C/S_Y, a constant that reflects properties of the recording system and the fluorophores. S_C/S_Y can be determined from measurements of a donor–acceptor pair with a known E value or from a global fit of multiple datasets collected with the same recording system and the same fluorophores. After S_C/S_Y is determined, the FRET efficiency E can be determined by fitting Eqs. 1 and 2 to the data. We conducted model fitting in Microsoft Excel using the minimum chi-square method.

RESULTS

TRPV Expression in HEK Cells

To investigate TRPV subunit assembly, we tested thermosensitive TRPV subunit coassembly in live cells. Strong fluorescence was exhibited by HEK 293 cells that were transfected with fluorescently tagged TRPV subunits (Fig. 3 A). One noticeable feature of these cells was that fluorescence was observed from both the plasma membrane (Fig. 3 A, red arrow) and intracellular structures (Fig. 3 A, white arrow), similar to previous reports (Hellwig et al., 2005). The strong intracellular fluorescence signal may result from overexpression, trafficking defects, accumulation of partially degraded proteins, or other sources. We noticed that the intracellular fluorescence signal exhibited variability in spectral properties. In contrast, the plasma membrane–derived fluorescence signal was more homogenous, and its spectrum was comparable to that published for Cerulean (Rizzo et al., 2004) and eYFP (Heim and Tsien, 1996). Examples of the intracellular fluorescence signal and the plasma membrane–derived fluorescence signal, taken from the same cell, are shown in Fig. 3 B. As mature, properly assembled channels are most likely found in the plasma membrane, we used a "spectra FRET" approach to isolate and quantify the plasma membrane–derived fluorescence signal.

Spectra FRET Measurement from the Plasma Membrane

We measured fluorescence emission spectra under an epifluorescence microscope using a combination of a spectrograph and a CCD camera. The image of a fluorescent cell was projected onto the input slit of the spectrograph that was attached to the side port of the microscope (Fig. 4, A and D). The fluorescence from the cell portion covered by the slit was in turn projected onto the CCD camera attached to the output port of the spectrograph. The projected image was shifted laterally on the CCD camera by the grating of the spectrograph; the amount of shift depended on the wavelength of the

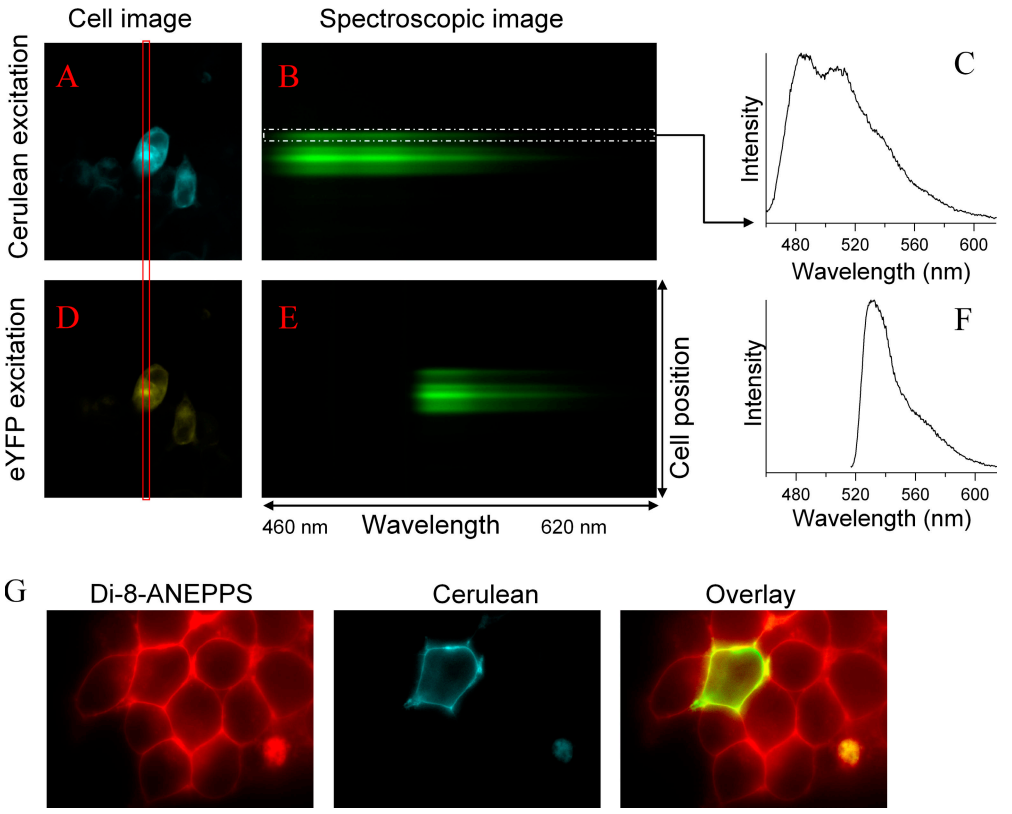

Figure 4. Spectra FRET. A single HEK 293 cell co-expressing TRPV3_Cerulean and TRPV3_eYFP was observed with CFP (A) or YFP (D) excitation. Spectroscopic images from the region under the slit (indicated by the rectangle) were recorded with each excitation (B and E). In the spectroscopic images, the Y axis represents the position of the cell, the X axis represents the wavelength. The fluorescence intensity values measured from the upper membrane region (indicated by a box) are shown in C and F. Notice the bright strips in B and E between the membrane signals, which represent fluorescence from intracellular sources. (G) Co-localization of di-8-ANEPPS, a plasma membrane marker fluorophore (red, left), and TRPV2_Cerulean (cyan, middle). In the overlay image (right), Cerulean fluorescence is shown in green.

emission light. This resulted in a spectroscopic image in which the Y axis represented the position of the cell portion visible through the slit, and the X axis represented the wavelength (Fig. 4, B and E). As the position of the cell is preserved in the Y dimension of each spectroscopic image, fluorescence signals from the plasma membrane and those from intracellular sources can be easily distinguished. Quantifying the fluorescence intensity along the X axis yielded the emission spectrum. In the present study, all the fluorescence measurements (except mentioned specifically) were made from the plasma membrane.

To confirm that the plasma membrane–derived fluorescence signals could be reliably identified, we labeled transfected cells with di-8-ANEPPS, a red fluorescent dye that bound specifically to the outer leaflet of the plasma membrane and served as a marker for the plasma membrane. As shown in Fig. 4 G, we observed significant overlay between the di-8-ANEPPS fluorescence and the TRPV2_Cerulean fluorescence. This indicates that fluorescently tagged TRPV channels were indeed expressed in the plasma membrane and the fluorescence signal from this population of channels could be reliably identified by the spectra FRET approach.

To measure FRET from cells transfected with a pair of TRPV subunits labeled with Cerulean and eYFP, respectively, we took two spectroscopic images, one with the Cerulean excitation at 436 nm (Fig. 4 B) and another with the eYFP excitation at 500 nm (Fig. 4 E). From these two images, we constructed the total emission spectrum and the YFP emission spectrum, respectively (Fig. 4, C and F). Similar emission spectra were collected from cells expressing only Cerulean-tagged subunits or only eYFP-tagged subunits. Based on these spectral measurements, the FRET efficiency was calculated as the enhanced eYFP emission due to energy transfer.

FRET in Homomeric TRPV Channels

Using the approach outlined above we first recorded FRET from homomeric TRPV channels. As the tetrameric subunit arrangement of TRPV channels brought Cerulean and eYFP into the same channel complex, these positive controls served two purposes: (1) they tested for the reliability of our FRET model, and (2) they provided a measure of the FRET efficiency range expected from these TRPV channels. Examples of these experiments are shown in Fig. 5, in which the FRET efficiency was calculated individually from a total of 59 cells coexpressing TRPV3_Cerulean and TRPV3_eYFP (Fig. 5 A), or from 64 cells coexpressing TRPV2_Cerulean and TRPV2_eYFP (Fig. 5 B). We plotted the FRET efficiency as a function of the fluorescence intensity ratio between Cerulean and eYFP. An interesting feature of the data is the clear correlation between the FRET efficiency value and the fluorescence intensity ratio: the FRET efficiency started low at low Fc/Fy values, rising sharply as Fc/Fy increased, and apparently approaching

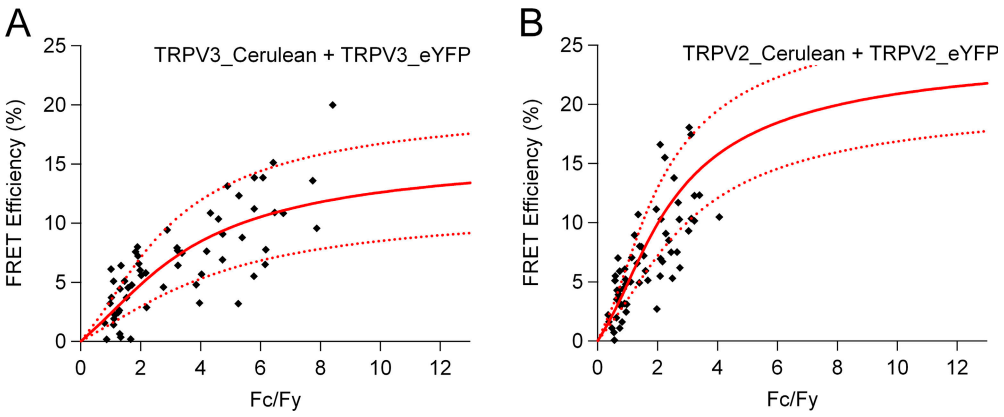

Figure 5. FRET measurements from homomeric TRPV channels. The FRET efficiency measured from cells expressing TRPV3_Cerulean/TRPV3_eYFP (A) or TRPV2_Cerulean/TRPV2_eYFP (B) is plotted as a function of the fluorescence intensity ratio between Cerulean and eYFP. Each symbol represents a single cell. The solid curve represents the FRET model that yields the best fit; dotted curves represent models with 5% higher or lower FRET efficiencies.

a plateau at high Fc/Fy values. As demonstrated in Fig. 2, the correlation between the FRET efficiency and Fc/Fy is what one would expect from a population of channels containing different numbers of Cerulean-containing subunits and eYFP-containing subunits. As the concentration ratio between the two subunit types changed (due to varying expression level), so did the distribution among channels with different subunit compositions. When eYFP-containing subunits were relatively abundant (low Fc/Fy), most of the channels contained multiple eYFP-containing subunits and none or one Cerulean-containing subunit. Those eYFP molecules that were not coupled to a Cerulean molecule contributed to the total eYFP intensity but not to the FRET signal, causing a reduction of the overall FRET efficiency. On the other hand, when Cerulean-containing subunits were abundant (high Fc/Fy), most eYFP molecules were coupled to one or multiple Cerulean molecules and contributed to FRET, yielding higher FRET seen in the data.

We fitted the data to our FRET model (see Materials and methods) to estimate the FRET efficiency between fluorophores on the neighboring subunits. FRET efficiencies of 8.4 and 13.5% yielded the best fit for TRPV3 and TRPV2 homomeric channels, respectively (Fig. 5, solid curves). Notice that when Cerulean and eYFP fluorescence intensities are equal (Fc/Fy = 1), the FRET efficiency is substantially lower, at only 2.4 and 4.9%, respectively. To evaluate the confidence range of our FRET estimate, we also tried to fit the data with an efficiency value that was either 5% higher or lower than the estimated FRET efficiency (Fig. 5, dotted curves). As shown in Fig. 5, most of the data points fall between the two dotted curves, suggesting that our FRET measurements had errors $<\pm 5\%$.

Comparable FRET signals were also observed from the other two homomeric TRPV channels (Table II). The FRET values again exhibited strong correlation to Fc/Fy, as predicted by the FRET model. The FRET efficiencies estimated from these channels are 11.3 and 18.1% for TRPV1 and TRPV4, respectively. Results from homomeric TRPV channels thus confirmed that FRET could be used to reliably report TRPV subunit coassembly in live cells.

Absence of FRET in Cells Coexpressing Unrelated Channel Subunits

When fluorescently tagged TRPV subunits are expressed at high density, it is possible that nonspecific FRET would occur between neighboring channel proteins. To distinguish between FRET within the same channel and possible nonspecific FRET between fluorophores in different channels that happened to be in close proximity, we coexpressed fluorescently tagged TRPV with unrelated ion channel proteins, including TRPM4, TRPM5, and CLC-0, that had been tagged with the complementary fluorophore. As most of these constructs expressed at least as well as the TRPVs, FRET measurements from these cells provide a reliable estimate of the nonspecific FRET level. An example dataset from these experiments is shown in Fig. 6 A, in which cells coexpressing CLC-0_Cerulean and TRPV2_eYFP were tested ($n = 62$). The FRET values from these cells were very low even at high Fc/Fy ratios where we observed robust FRET from homomeric TRPV channels. As expected, our FRET model fitted the data from these negative experiments very poorly, with an apparent Evalue $<4.5\%$. Similar results were found when TRPV2_Cerulean and TRPM5_eYFP (Fig. 6 B, $n = 25$), TRPM4_Cerulean and TRPV2_eYFP ($n = 16$; unpublished data), or TRPM5_Cerulean and TRPV2_eYFP ($n = 17$; unpublished data) were coexpressed, even though TRPM4 and TRPM5 are more closely related to the TRPV channels. Closer inspection, however, did reveal a positive, though very weak, correlation between the FRET efficiency and Fc/Fy. Such correlation might come from nonspecific energy transfer between neighboring channel proteins due to high expression (Takanishi et al., 2006). A linear fit yielded a slope factor of 0.52 for CLC-0_Cerulean/TRPV2_eYFP coexpression and 0.37

TABLE II

Summary of FRET Efficiency Measurements

	TRPV1_eYFP	TRPV2_eYFP	TRPV3_eYFP	TRPV4_eYFP
TRPV1_Cerulean	11.3% (0.013) $n = 62$	12.8% (0.008) $n = 31$	6.7% (0.011) $n = 67$	7.7% (0.011) $n = 79$
TRPV2_Cerulean	10.6% (0.018) $n = 69$	13.5% (0.012) $n = 64$	8.7% (0.016) $n = 58$	9.0% (0.023) $n = 32$
TRPV3_Cerulean	11.1% (0.011) $n = 24$	10.9% (0.019) $n = 110$	8.4% (0.011) $n = 59$	7.6% (0.013) $n = 67$
TRPV4_Cerulean	9.4% (0.009) $n = 30$	7.5% (0.014) $n = 56$	9.9% (0.018) $n = 32$	18.1% (0.027) $n = 81$

The FRET efficiency value is determined by fitting the FRET model to each coexpression experiment and is given as a percentage; the number in parentheses represents the mean chi-square value for the best fit; n represents the number of cells.

for TRPV2_Cerulean/TRPM5_eYFP coexpression (Fig. 6), suggesting that contaminations due to nonspecific FRET under our experimental conditions were minor.

FRET in Heteromeric TRPV Channels

The experiments described above established that spectra FRET can be reliably applied to transfected cells. Using this spectra FRET approach, we systematically measured FRET efficiencies from cells coexpressing different TRPV subunit pairs. The results are summarized in Table II; representative data are shown in Fig. 7. FRET efficiency from all these experiments exhibited strong correlation to the ratio Fc/Fy. Fitting the data to our FRET model yielded FRET efficiency estimates that ranged from 6.7 to 12.8%. These results were comparable to those of the homomeric channels. The agreement between the model and the data, judging from either the confidence range or the mean chi-square value, was also comparable to that of the homomeric channels.

Closer examination of the data supported the notion that genuine FRET signals were observed from cells coexpressing different TRPV subunits. For example, the highest mean chi-square value, measured from the TRPV2_Cerulean/TRPV4_eYFP dataset (Fig. 7 D), appeared to be mostly due to a few points at high Fc/Fy ratios, where Fy is generally very low and hard to quantify. Furthermore, even the dataset with the lowest FRET estimate, from TRPV1_Cerulean/TRPV3_eYFP (Fig. 7 C), exhibited a clear positive correlation between the FRET efficiency and Fc/Fy that was distinctive from the negative control experiments (see above). We did notice that a subset of cells in this and some other measurements appeared to exhibit a lower FRET efficiency that could not be accounted for by the FRET model (see also Fig. 5, A and B). The origin of this subpopulation is currently unclear. Hellwig and colleagues examined TRPV expression in HEK 293 cells with confocal microscopy and found that different TRPV subunits tended to localize differently (Hellwig et al., 2005). If differential localization of Cerulean- and eYFP-containing channels also existed under our experimental conditions, it would account for the reduction in the FRET efficiency.

A direct comparison between FRET efficiencies from coexpression of different subunits and those from homomeric TRPV channels is shown in Fig. 8, in which the FRET efficiency is plotted as a function of the sequence similarity between each subunit pair. A dotted line is drawn at 8.4%, which corresponds to the lowest FRET level among all homomeric channels; most of the FRET values from coexpression experiments are above this level. In addition, every TRPV subunit we tested yielded FRET above this level in some, if not all, of the combinations. FRET values measured from all the TRPV subunit combinations are substantially higher then the background, nonspecific FRET level. We thus conclude that temperature-sensitive TRPV subunits do coassemble to form heteromeric channels.

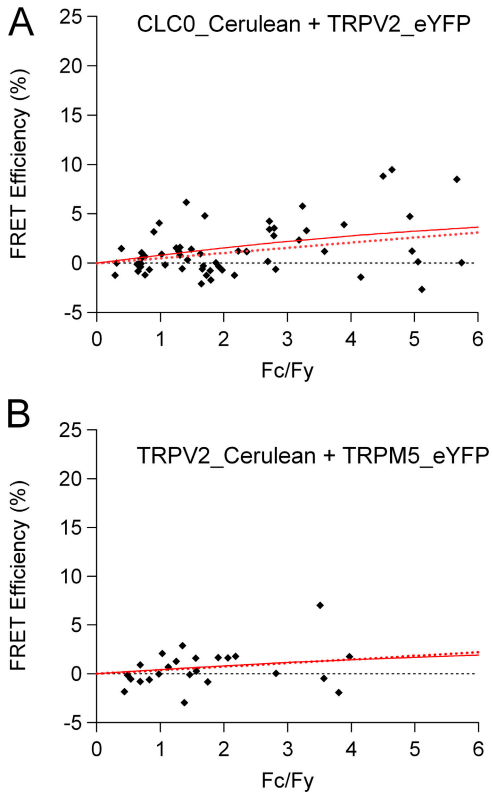

Figure 6. Measurements from cells coexpressing CLC-0_Cerulean/TRPV2_eYFP (A) and TRPV2_Cerulean/TRPM5_eYFP (B), which serve as negative controls. The dotted lines represent a linear fit to the dataset; the solid curves represent fits of the FRET model to the dataset.

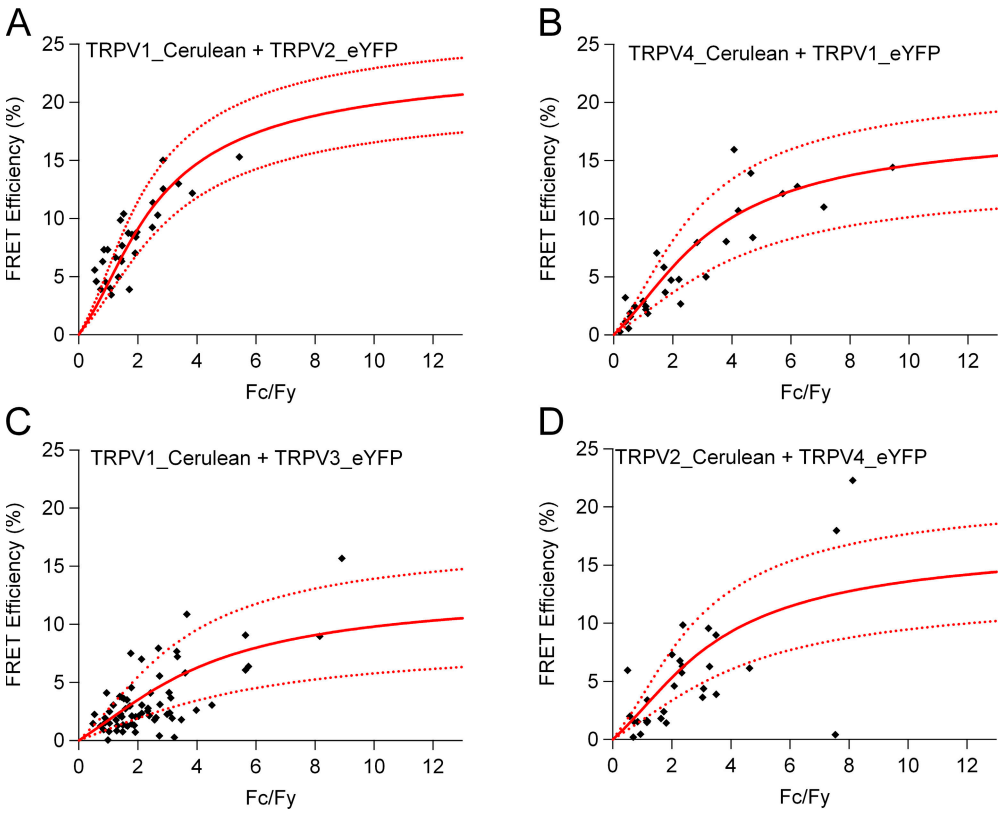

Figure 7. FRET measurements from heteromeric TRPV channels. The FRET efficiency measured from cells expressing TRPV1_Cerulean/TRPV2_eYFP (A), TRPV4_Cerulean/TRPV1_eYFP (B), TRPV1_Cerulean/TRPV3_eYFP (C), and TRPV2_Cerulean/TRPV4_eYFP (D) is plotted as a function of the fluorescence intensity ratio between Cerulean and eYFP. Each symbol represents a single cell. The solid curve represents the FRET model that yields the best fit; dotted curves represent models with 5% higher or lower FRET efficiencies.

FRET Signals Are Limited to the Plasma Membrane

Our spectroscopy experiments suggested that TRPV subunits coassembled into heteromeric channels that gave rise to strong FRET signals. However, a previous study of TRPV channels did not yield appreciable FRET for most of the subunit pairs (Hellwig et al., 2005). One noticeable difference between these two studies is that the previous study measured FRET from a region of the cell that covered both the plasma membrane and the intracellular area, while we focused specifically on the plasma membrane. As most of the TRPV protein-expressing cells exhibited strong intracellular fluorescence signal (Fig. 3 A), we suspected that the previous study's measurements would be heavily weighted by the intracellular signal, which showed substantially different spectral properties (Fig. 3 B). To test whether this was indeed the case, we selectively measured FRET from the intracellular region and compared it to the FRET measurement from the plasma membrane of the same cell. Examples from 13 cells coexpressing TRPV2_Cerulean and TRPV3_eYFP are shown in Fig. 9. The FRET estimate from the plasma membrane of this small group of cells (10.1%, solid red curve) was similar to that from a larger pool of cells (8.7%, $n = 58$) shown in Table II. However, the intracellular fluorescence signal clearly exhibited a much reduced FRET (5.5%, dotted red curve) that is only marginally higher than the background nonspecific FRET (3.5%, black curve). The difference between the intracellular FRET and the nonspecific FRET, 2%, is very similar to the FRET values that Hellwig and colleagues (2005) reported.

Single-Channel Recordings Identified Heteromeric TRPV Channels with Intermediate Conductance and Gating Properties

The FRET experiments described above indicate that a substantial fraction of channels in the plasma membrane of coexpressed cells are heteromeric. To directly observe these channels, we conducted single-channel

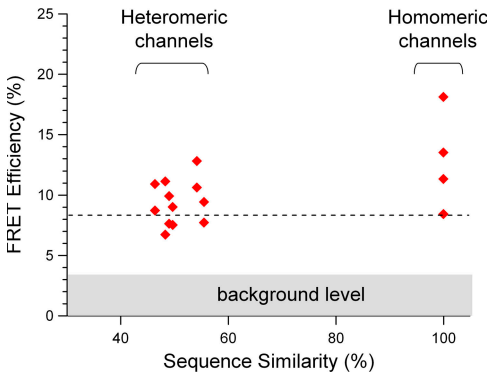

Figure 8. The relationship between the FRET efficiency and the sequence similarity. The dotted line, at the 8.4% level, corresponds to the lower boundary of the FRET efficiency range for the homomeric channels. The gray area represents the background level of nonspecific FRET.

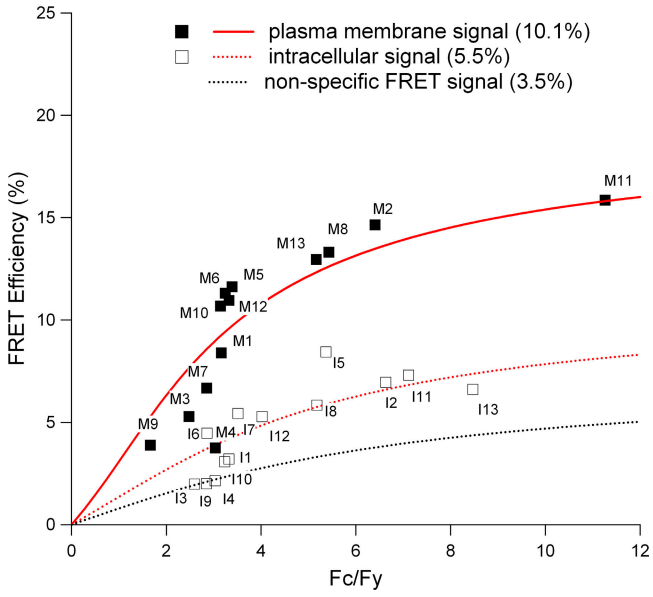

Figure 9. FRET detected from the plasma membrane. For each cell, FRET was estimated from both the plasma membrane (solid symbols) and the intracellular region (open symbols) and labeled as Mn and In, respectively, where n represents the cell identification number. The red solid and dotted curves represent the fit of the FRET model to the two datasets, respectively. The black dotted curve represents the background level, as seen in Fig. 6 A.

recordings from cells coexpressing two types of TRPV subunits to study the properties of heteromeric TRPV channels, and compared the results to those from homomeric TRPV channels. For this study, we chose to focus on TRPV1 and TRPV3, whose single-channel behavior is very different from each other.

Fig. 10 A shows single-channel current traces recorded from a TRPV1 channel expressed in HEK 293 cells. TRPV1 current exhibited long openings that were interrupted by flickering closures. All-point histograms were built from these single-channel records (Fig. 10 B). The single-channel conductance, measured at +80 mV, was estimated to be 61.9 ± 11.7 pS (n = 6), similar to previously reported values estimated in *Xenopus* oocytes (Hui et al., 2003). As shown in Fig. 10 (A and B), TRPV1 current exhibited strong outward rectification, which is a hallmark for TRPV channels (Clapham et al., 2001).

To better characterize the gating properties of TRPV1, we used HMM to estimate the gating transition rates near steady state at +80 mV. As single-channel recordings clearly revealed long closures between openings as well as brief closures within openings, we chose to use a simple C↔O↔C model. The model appeared to adequately predict the single-channel behavior of TRPV1 (Fig. 10 C). The HMM analysis showed that, at +80 mV, the mean life-time in the open state is 16.2 ms, while the mean life-times for the long and short closed states are 26.0 and 1.4 ms, respectively. The mean burst duration was estimated to be 53.5 ms. These results are, again, in agreement with previous reports on TRPV1 channels (Hui et al., 2003; Ryu et al., 2003).

The TRPV3 single-channel current exhibited clear differences from TRPV1 current. As shown in Fig. 11, the single-channel conductance of TRPV3 at +80 mV was estimated to be 158.3 ± 30.2 pS (n = 3), nearly three times higher than that of TRPV1. Similar to TRPV1 current, TRPV3 current was also outwardly rectifying (Fig. 11, A and B). However, the current rectification was apparently weaker in TRPV3 channel; the ratio between the current amplitude at +80 mV and the current amplitude at +40 mV was 2.8 for TRPV1 and 1.6 for TRPV3. Furthermore, the opening of TRPV3 was substantially briefer. At +80 mV, the mean burst duration of TRPV3 current was estimated to be 14.8 ms (Fig. 11 C), almost four times shorter than that of TRPV1 current.

The dramatic differences between TRPV1 and TRPV3 single-channel currents suggest that heteromeric channels formed between the TRPV1 subunit and the TRPV3 subunit should exhibit distinguishable properties from both parental channel types. A total of 37 single-channel recordings were made from cells coexpressing TRPV1 and TRPV3 subunits. As expected, we recorded five channels that exhibited the phenotype of homomeric TRPV1 channel. These channels had very long openings and a low conductance; the mean conductance at +80 mV was estimated as 57.9 ± 1.5 pS. We also recorded one channel that exhibited the phenotype of homomeric TRPV3 channel, with high conductance and brief openings. The single channel conductance at +80 mV was measured to be 177.1 pS for this channel. In addition, we observed 31 channels with intermediate conductance and gating properties. Currents from these channels are clearly distinct from the occasional endogenous channel activities observed from untransfected cells. Fig. 12 shows example single-channel traces and all-point histograms from one such channel. In this case, the single-channel conductance, estimated at 77.3 pS, fell between that of TRPV1 homomer and TRPV3 homomer. In addition, the life-time in the open level appeared to be also between that of the two homomeric channel types. The mean burst time was estimated with HMM to be 24.0 ms. These phenotypes suggest that the channel might be composed of both TRPV1 subunits and TRPV3 subunits.

All the channels having intermediate conductances and gating properties can be grouped into four populations with single-channel conductance values of 66.6 ± 0.7 pS (n = 16), 78.1 ± 1.0 pS (n = 10), 98.8 ± 2.6 pS (n = 4), and 131.7 pS (n = 1). Examples of single-channel currents at +80 mV and an all-point histogram for each group are shown in Fig. 13. A noticeable trend is that channels with relatively low conductance had longer openings (similar to TRPV1 channels), while channels with relatively higher conductance had shorter openings

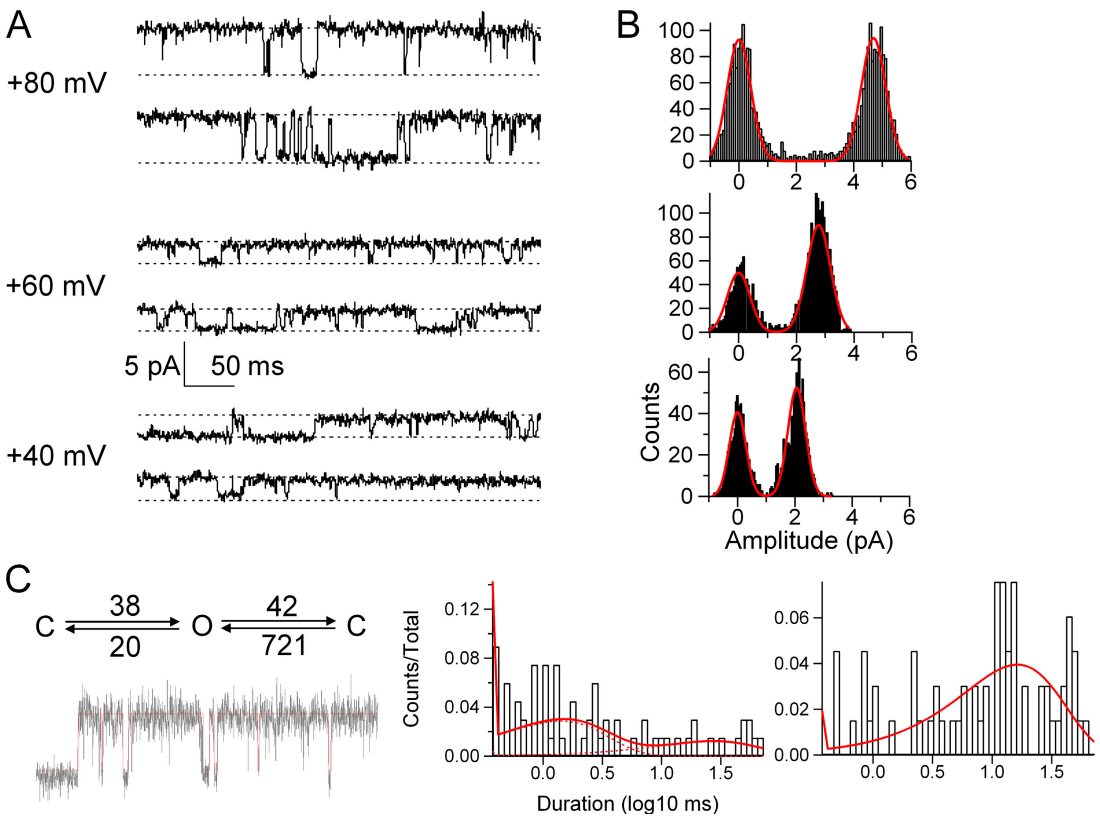

Figure 10. TRPV1 homomeric channels. (A) Representative single-channel traces recorded at +80, +60, and +40 mV. (B) All-point histograms at each voltage. The red curves are fits of a double-Gaussian function. (C, left) A kinetic model used in hidden Markov modeling analysis of the gating properties, with transition rates, in s^{-1}, determined from single-channel recordings at +80 mV. The burst duration calculated from this model is 14.8 ms. Also shown is a representative single-channel trace with idealization (red) overlaid on top. (C, middle, right) Histograms of the closed and open durations. Curves are fits of Gaussian functions.

(similar to TRPV3 channels) (Fig. 13 A). The correlation between conductance and gating strongly suggests that channels of different groups may have different subunit stoichiometry; a higher number of TRPV1 subunits made the channel behave more like TRPV1 channels, and vice versa. Based on this assumption, we tentatively assigned the subunit stoichiometry for each group of channels, as shown in Fig. 13.

Distribution of TRPV Heteromeric Channel Types

If we assume that TRPV1 and TRPV3 subunits can co-assemble randomly into tetramers, the frequency of recording channels having each stoichiometry should follow a binomial distribution. Fig. 14 summarizes the frequency with which we observed channels that appeared to belong to each channel type. The data could be fitted reasonably well to a binomial function. The fit yielded a higher probability of observing a TRPV1 subunit (65.5%) over a TRPV3 subunit. This is to be expected from the way we chose cells for patch recording: in these experiments, TRPV1_Cerulean and TRPV3_eYFP were coexpressed and the Cerulean emission from individual cells was used as indication of positive expression. As this selection method only ensured the presence of TRPV1 but not TRPV3 in the recorded cells, a higher probability of observing TRPV1 subunit–containing channels is expected. The reasonable agreement between the frequency data and the binomial function fit suggests that coassembly between the TRPV1 subunit and the TRPV3 subunit are likely to be near random. This finding is consistent with the FRET experiments described above in which the FRET distribution also indicated random subunit assembly.

In summary, single-channel recordings revealed four types of heteromeric TRPV channels. The intermediate conductance and gating properties of these channel types are consistent with them having varying numbers of different TRPV subunits.

DISCUSSION

In the present study, we tested the ability of thermosensitive TRPV channel subunits to form heteromeric channels. Two complementary approaches were used to measure specifically from the plasma membrane where mature, functional channels are expected to be located. Using a spectra FRET approach, we observed positive FRET signals between most TRPV subunit pairs in live

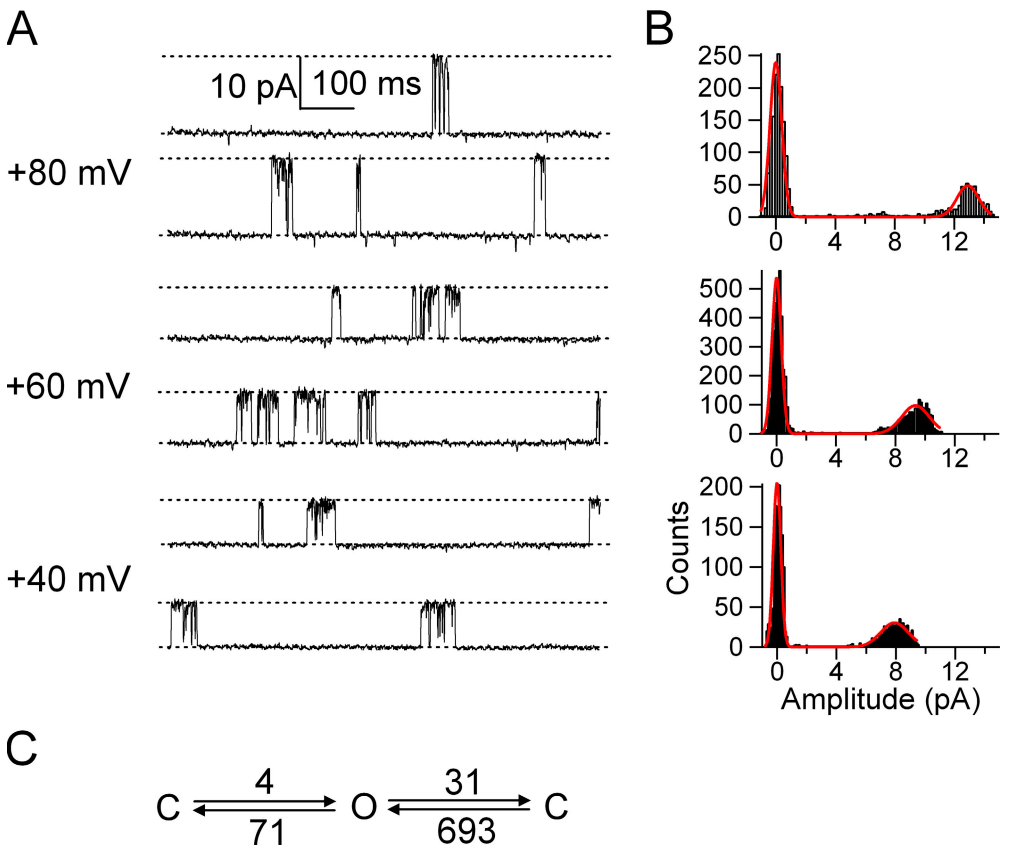

Figure 11. TRPV3 homomeric channels. (A) Representative single-channel traces recorded at +80, +60, and +40 mV. (B) All-point histograms at each voltage. The red curves are fits of a double-Gaussian function. (C) A kinetic model used in HMM analysis of the gating properties. The burst duration calculated from this model is 53.5 ms.

cells. This finding was further supported by experiments using homomeric TRPV channels, which exhibited very similar FRET behavior to the heteromeric channels, as well as by experiments using coexpression of TRPV subunits with nonrelated channel subunits such as TRPM channels and CLC-0 chloride channels, which exhibited only very weak nonspecific FRET. The latter result suggested that the FRET signals were not artifacts due to overexpression of these subunits in culture cells. Single-channel recordings further confirmed the formation of heteromeric TRPV channels and revealed dramatic differences in functional properties between homomeric channels and heteromeric channels. Our results confirmed previous reports of heteromeric channel formation between specific TRPV subunits (Smith et al., 2002; Tobin et al., 2002; Liapi and Wood, 2005; Rutter et al., 2005) and are consistent with observations of heteromeric channel formations within other TRP subfamilies (for review see Schaefer, 2005).

TRPV Subunit Coassembly

Heteromeric channel formation by TRPV subunits may not be totally surprising. TRP channels are grouped by sequence similarities into TRPC, TRPV, TRPM, etc. Heteromeric channel formation has been widely reported for subunits within the TRPC and TRPM subfamilies (Xu et al., 1997; Lintschinger et al., 2000; Xu et al., 2000; Strubing et al., 2001; Goel et al., 2002; Hofmann et al., 2002; Amiri et al., 2003; Strubing et al., 2003; Chubanov et al., 2004; Liu et al., 2005; Li et al., 2006; Poteser et al., 2006). It appears that, in general, coassembly tends to occur between subunits with high sequence similarities (Schaefer, 2005). The sequence similarities between TRPV subunits are comparable to those of the TRPC subunits or the TRPM subunits that do form heteromeric channels.

How TRP subunits recognize and interact with each other is still poorly understood, though specific interactions mediated by domains within the high sequence similarity regions are likely to be important. It has been suggested that regions of the N terminus (Erler et al., 2004; Arniges et al., 2006; Vos et al., 2006) and the C terminus (Garcia-Sanz et al., 2004) may play an important role in TRPV subunit–subunit interactions. All of the TRPV subunits in this study contain multiple ankyrin repeats in the N-terminal intracellular region. Ankyrin repeats form well-defined structures that constitute a widely distributed protein–protein interaction domain (Jin et al., 2006; McCleverty et al., 2006). Most of ankyrin-mediated interactions reported so far are found between the ankyrin repeat domain and a nonankyrin structure (for review see Mosavi et al., 2004). The intracellular C terminus of TRPV1 has been proposed to resemble the corresponding region of the hyperpolarization-activated, cyclic nucleotide-regulated (HCN) channels (Garcia-Sanz et al., 2004). For HCN channels and

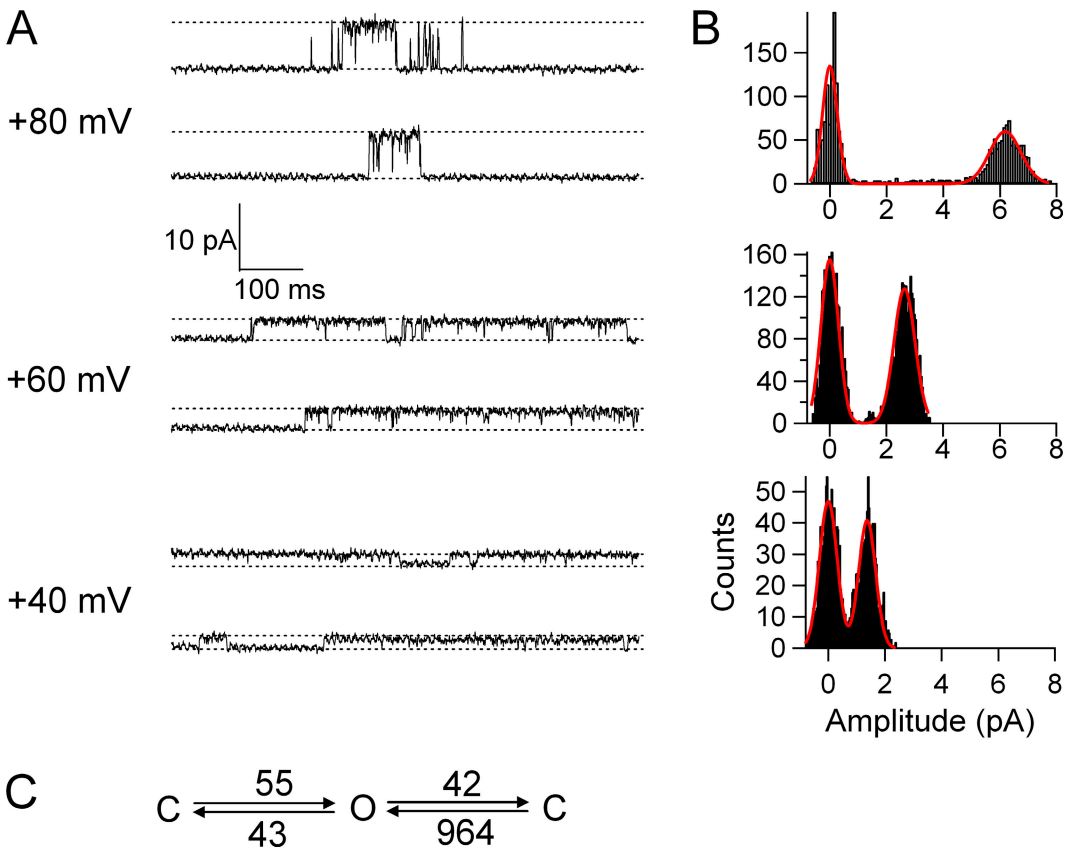

Figure 12. Representative heteromeric channel formed with TRPV1 and TRPV3 subunits. (A) Representative single-channel traces recorded at +80, +60, and +40 mV. (B) All-point histograms at each voltage. The red curves are fits of a double-Gaussian function. (C) A kinetic model used in HMM analysis of the gating properties. The burst duration calculated from this model is 24.0 ms.

related cyclic nucleotide-gated channels, the intracellular C terminus has been shown to mediate subunit–subunit interactions (Gordon and Zagotta, 1995; Johnson and Zagotta, 2001; Rosenbaum and Gordon, 2002; Zagotta et al., 2003; Hua and Gordon, 2005). It remains to be tested whether interactions between TRPV subunits are mediated by similar regions. Our present study showed that coassembly occurred between most TRPV subunits, and the assembly did not appear to follow fixed stoichiometry. These results indicate that the structure (s) mediating subunit interaction is likely common to all thermosensitive TRPV subunits.

Spectra FRET

Hellwig and colleagues have previously studied TRPV subunit coassembly (Hellwig et al., 2005). The experimental conditions in that study were in many ways very similar to ours. For example, in their study mouse TRPV clones were tagged with fluorescent proteins at the C terminus and the fusion proteins were coexpressed in HEK 293 cells. We also studied C terminus–tagged mouse clones in HEK cells. Both studies used the FRET approach. However, the previous study observed subunit coassembly only between TRPV1 and TRPV2 (as well as between TRPV5 and TRPV6, which were not included in the present study). What, then, caused the discrepancy between these two studies? Besides obvious methodological differences—for example, in the previous study FRET between the original cyan fluorescent protein and yellow fluorescent protein was quantified by the increase in donor emission after photobleaching the acceptor—a noticeable difference is the way fluorescence signal was collected.

In the previous study, fluorescence from a rectangular region of the cell was analyzed (Hellwig et al., 2005). We used a spectroscopic imaging approach, "spectra FRET," to selectively record fluorescence signal from the plasma membrane. As we have demonstrated in the present study (Fig. 9), including intracellular fluorescence may cause the absence of FRET. Both the previous report by Hellwig and colleagues and our own observation (Fig. 3 A) showed that a large portion of the expressed TRPV subunits stayed inside the cell, probably due to missing proteins that normally interact with TRP channels (Cuajungco et al., 2006). As subunits trapped inside the cell might not exist as parts of properly formed channels or in similar cellular environment as the plasma membrane, we chose to exclude them from our analysis. Our decision was based on two lines of evidence. First, we observed a significant difference

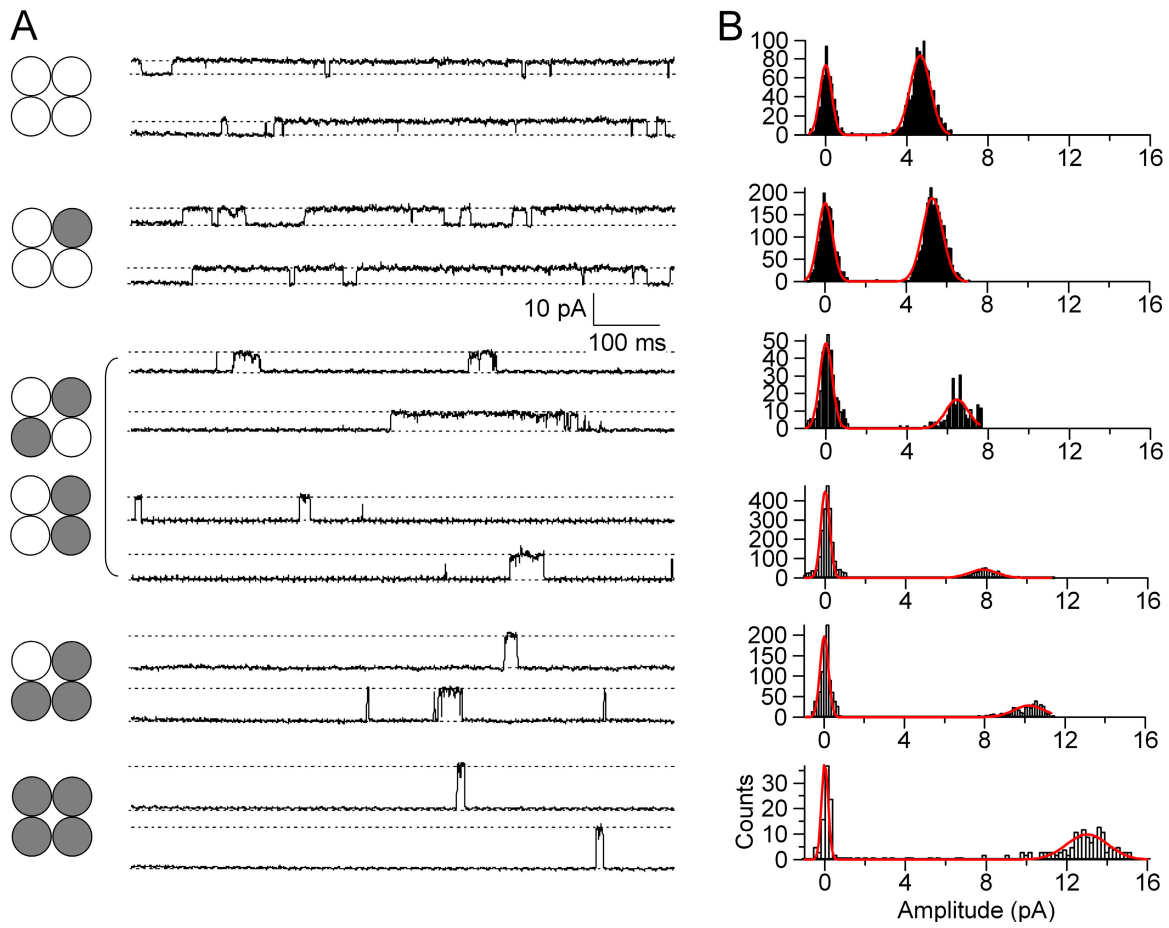

Figure 13. Comparison of homomeric and heteromeric TRPV channels. (A) Representative current traces recorded at +80 mV from cells cotransfected with TRPV1 and TRPV3. (B) All-point histograms constructed from single-channel recordings of each channel type. The red curves are fits of a double-Gaussian function. Shown on the left are possible subunit stoichiometries; open and filled circles represent the TRPV1 and TRPV3 subunits, respectively.

between the fluorescence signal originating from the intracellular structures and that from the plasma membrane (Fig. 3 B). The cause of such difference is not clear; fluorophore aggregation, exposure of the fluorophore to different local cellular environments, and contribution from nascent, immature as well as partially degraded fluorescent proteins may all contribute to fluorescence variability. Second, different TRPV subunits appeared to distribute at distinct intracellular locations. Hellwig and colleagues characterized the subcellular localization of the expressed TRPV subunits with confocal microscopy (Hellwig et al., 2005). They concluded that, overall, different TRPV subunits were not colocalized. Different subcellular localizations would contribute to the absence of FRET, as FRET requires the fluorophore pair to be much closer than the optical resolution limit (hundreds of nanometers).

Separation of the fluorescence signal in the plasma membrane from those of the intracellular structures was achieved in the present study with a spectra FRET approach. We achieved spectra FRET functionality on a fluorescence microscopy system through the addition of a spectrograph/CCD camera unit. A spectrograph is currently available in various configurations, allowing easy attachment to most microscope brands. As the spectroscopy measurement preserved both the spectral information and the spatial information (Bykova et al., 2006; Takanishi et al., 2006; Zheng, 2006), fluorescence signals from the plasma membrane as well as other cellular structures could be conveniently identified.

The correlation between the FRET efficiency and the fluorescence intensity ratio between Cerulean and eYFP (Fc/Fy) observed in this study highlights another important factor for FRET experiments under similar experimental conditions. In all of our measurements the FRET efficiency was very low at low Fc/Fy values, reaching the plateau phase only at high Fc/Fy values. This characteristic correlation is correctly predicted by our FRET model (Fig. 2), and is most likely due to highly variable expression levels of Cerulean and eYFP in individual cells. It underlines the importance of determining FRET efficiency with cells in a wide Fc/Fy range. The model shown in Fig. 2 C indicates that FRET efficiency would be substantially underestimated if the

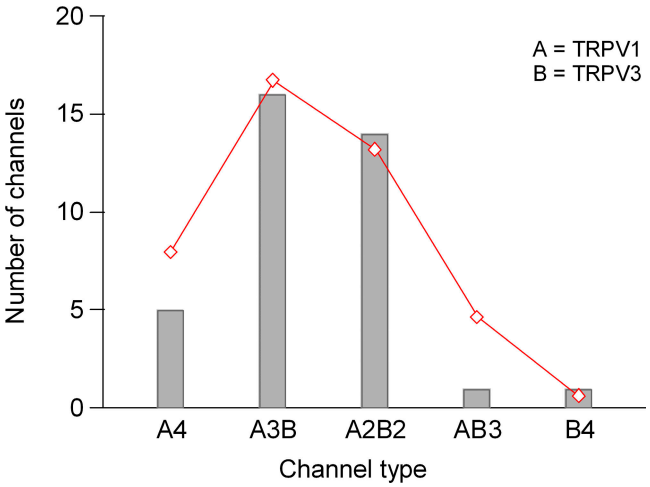

Figure 14. The frequency of recording each channel type from cells cotransfected with TRPV1 and TRPV3. Superimposed is a fit of a binomial function, with the probability of incorporating a TRPV1 subunit being 65.5%.

measurement is limited to cells having equal Cerulean and eYFP signals (Fc/Fy = 1). Similar precautions were taken in the study by Hellwig and colleagues, in which only cells exhibiting high Fc/Fy were used (Hellwig et al., 2005), as well as by many other investigators (Erickson et al., 2001; Amiri et al., 2003).

Implications of TRPV Channel Functions

Our results confirmed that thermosensitive TRPV subunits do coassemble into heteromeric channels that exhibit significantly different functional properties. Studies of the cellular distribution of TRPV subunits suggest that heteromeric TRPV channels may also form in native cells (Tobin et al., 2002; Liapi and Wood, 2005). Expression of thermosensitive TRP channels in sensory neurons is found to overlap extensively. For example, within dorsal root ganglia, TRPV1, TRPV3, and the two cold-sensitive channels TRPM8 and TRPA1 are all expressed in small diameter, unmyelinated or lightly myelinated sensory neurons that also express peptide markers for nociceptors, such as calcitonin gene-related peptide (CGRP). Interestingly, the noxious cold-activated TRPA1 channel is found exclusively in neurons expressing the heat-activated TRPV1 channel (McKemy et al., 2002). Coexpression of multiple TRP subunit types is also found in other parts of the nervous system including spiral and vestibular ganglia (Kitahara et al., 2005), vagal afferent neurons (Zhang et al., 2004), as well as many other nonneuronal tissues (Heiner et al., 2003; Vriens et al., 2004; Kitahara et al., 2005).

Humans possess exquisite thermosensitivity that allows us to detect temperature differences as small as a single degree. The molecular mechanism through which high temperature sensitivity is achieved remains elusive. An intriguing hypothesis speculates that enhanced temperature sensitivity may come in part from the formation of heteromeric channels by thermosensitive TRPV subunits (Jordt et al., 2003; Moran et al., 2004). Besides expressing at high levels in dorsal root ganglia neurons that receive sensory input from the periphery, TRPV1–4 are also found to be broadly expressed in other tissues including heart and brain that normally sustain stable temperature, suggesting that these channels may serve other important functional roles (Caterina and Julius, 2001; Clapham, 2003). The formation of heteromeric TRPV channels has many intriguing implications regarding both temperature sensing and other physiological functions in which these channels participate.

We are grateful to the following colleagues for their generous gifts of various constructs: Drs. Michael Xi Zhu (TRPV1; Ohio State University, Columbus, OH), Itaru Kojima (TRPV2; Gunma University, Maebashi, Japan), Ardem Patapoutian (TRPV3; University of California, San Diego, CA), Sharona Gordon (TRPV3; University of Washington, Seattle, WA), Veit Flockerzi and Ulrich Wissenbach (TRPV4; Universität des Saarlandes, Homburg, Germany), Emily Liman (TRPM4 and TRPM5; University of Southern California, Los Angeles, CA), Tsung-Yu Chen (CLC-0; University of California, Davis, CA), David Piston (Cerulean; Vanderbilt University, Nashville, TN), and Roger Tsien (eYFP; University of California, San Diego, CA). We also thank Dr. Edward Lachica (Olympus) for support of the Spectra FRET imaging system, Ekaterina Bykova for helpful discussions, Drs. Sharona Gordon, and Stephen Adams (University of California, San Diego, CA) for critical reading of the manuscript, and Erica Whitney for her kind help with the language.

This work was supported by an award from the American Heart Association (0665201Y) to J. Zheng.

Olaf S. Andersen served as editor.

Submitted: 3 January 2007
Accepted: 2 February 2007

REFERENCES

Ahluwalia, J., H. Rang, and I. Nagy. 2002. The putative role of vanilloid receptor-like protein-1 in mediating high threshold noxious heat-sensitivity in rat cultured primary sensory neurons. *Eur. J. Neurosci.* 16:1483–1489.

Amiri, H., G. Schultz, and M. Schaefer. 2003. FRET-based analysis of TRPC subunit stoichiometry. *Cell Calcium.* 33:463–470.

Arniges, M., J.M. Fernandez-Fernandez, N. Albrecht, M. Schaefer, and M.A. Valverde. 2006. Human TRPV4 channel splice variants revealed a key role of ankyrin domains in multimerization and trafficking. *J. Biol. Chem.* 281:1580–1586.

Bykova, E.A., X.-D. Zhang, T.-Y. Chen, and J. Zheng. 2006. Large movement in the C terminus of CLC-0 chloride channel during slow gating. *Nat. Struct. Mol. Biol.* 13:1115–1119.

Caterina, M.J., and D. Julius. 2001. The vanilloid receptor: a molecular gateway to the pain pathway. *Annu. Rev. Neurosci.* 24:487–517.

Caterina, M.J., A. Leffler, A.B. Malmberg, W.J. Martin, J. Trafton, K.R. Petersen-Zeitz, M. Koltzenburg, A.I. Basbaum, and D. Julius. 2000. Impaired nociception and pain sensation in mice lacking the capsaicin receptor. *Science.* 288:306–313.

Caterina, M.J., T.A. Rosen, M. Tominaga, A.J. Brake, and D. Julius. 1999. A capsaicin-receptor homologue with a high threshold for noxious heat. *Nature.* 398:436–441.

Caterina, M.J., M.A. Schumacher, M. Tominaga, T.A. Rosen, J.D. Levine, and D. Julius. 1997. The capsaicin receptor: a heat-activated ion channel in the pain pathway. *Nature.* 389:816–824.

Chubanov, V., S. Waldegger, M. Mederos y Schnitzler, H. Vitzthum, M.C. Sassen, H.W. Seyberth, M. Konrad, and T. Gudermann. 2004. Disruption of TRPM6/TRPM7 complex formation by a mutation in the TRPM6 gene causes hypomagnesemia with secondary hypocalcemia. *Proc. Natl. Acad. Sci. USA.* 101:2894–2899.

Chung, M.K., H. Lee, and M.J. Caterina. 2003. Warm temperatures activate TRPV4 in mouse 308 keratinocytes. *J. Biol. Chem.* 278:32037–32046.

Clapham, D.E. 2003. TRP channels as cellular sensors. *Nature.* 426:517–524.

Clapham, D.E., C. Montell, G. Schultz, and D. Julius. 2003. International union of pharmacology. XLIII. Compendium of voltage-gated ion channels: transient receptor potential channels. *Pharmacol. Rev.* 55:591–596.

Clapham, D.E., L.W. Runnels, and C. Strubing. 2001. The TRP ion channel family. *Nat. Rev. Neurosci.* 2:387–396.

Clegg, R.M. 1992. Fluorescence resonance energy transfer and nucleic acids. *Methods Enzymol.* 211:353–388.

Cuajungco, M.P., C. Grimm, K. Oshima, D. D'Hoedt, B. Nilius, A.R. Mensenkamp, R.J. Bindels, M. Plomann, and S. Heller. 2006. PACSINs bind to the TRPV4 cation channel. PACSIN 3 modulates the subcellular localization of TRPV4. *J. Biol. Chem.* 281:18753–18762.

Dhaka, A., V. Viswanath, and A. Patapoutian. 2006. Trp ion channels and temperature sensation. *Annu. Rev. Neurosci.* 29:135–161.

Erickson, M.G., B.A. Alseikhan, B.Z. Peterson, and D.T. Yue. 2001. Preassociation of calmodulin with voltage-gated Ca^{2+} channels revealed by FRET in single living cells. *Neuron.* 31:973–985.

Erler, I., D. Hirnet, U. Wissenbach, V. Flockerzi, and B.A. Niemeyer. 2004. Ca^{2+}-selective transient receptor potential V channel architecture and function require a specific ankyrin repeat. *J. Biol. Chem.* 279:34456–34463.

Garcia-Sanz, N., A. Fernandez-Carvajal, C. Morenilla-Palao, R. Planells-Cases, E. Fajardo-Sanchez, G. Fernandez-Ballester, and A. Ferrer-Montiel. 2004. Identification of a tetramerization domain in the C terminus of the vanilloid receptor. *J. Neurosci.* 24:5307–5314.

Goel, M., W.G. Sinkins, and W.P. Schilling. 2002. Selective association of TRPC channel subunits in rat brain synaptosomes. *J. Biol. Chem.* 277:48303–48310.

Gordon, S.E., and W.N. Zagotta. 1995. A histidine residue associated with the gate of the cyclic nucleotide-activated channels in rod photoreceptors. *Neuron.* 14:177–183.

Guler, A.D., H. Lee, T. Iida, I. Shimizu, M. Tominaga, and M. Caterina. 2002. Heat-evoked activation of the ion channel, TRPV4. *J. Neurosci.* 22:6408–6414.

Heim, R., and R.Y. Tsien. 1996. Engineering green fluorescent protein for improved brightness, longer wavelengths and fluorescence resonance energy transfer. *Curr. Biol.* 6:178–182.

Heiner, I., J. Eisfeld, and A. Luckhoff. 2003. Role and regulation of TRP channels in neutrophil granulocytes. *Cell Calcium.* 33:533–540.

Hellwig, N., N. Albrecht, C. Harteneck, G. Schultz, and M. Schaefer. 2005. Homo- and heteromeric assembly of TRPV channel subunits. *J. Cell Sci.* 118:917–928.

Hille, B. 2001. Ion Channels of Excitable Membranes. Third edition. Sinauer Associates, Inc., Sunderland, MA. 814 pp.

Hofmann, T., M. Schaefer, G. Schultz, and T. Gudermann. 2002. Subunit composition of mammalian transient receptor potential channels in living cells. *Proc. Natl. Acad. Sci. USA.* 99:7461–7466.

Hua, L., and S.E. Gordon. 2005. Functional interactions between A' helices in the C-linker of open CNG channels. *J. Gen. Physiol.* 125:335–344.

Hui, K., B. Liu, and F. Qin. 2003. Capsaicin activation of the pain receptor, VR1: multiple open states from both partial and full binding. *Biophys. J.* 84:2957–2968.

Jahnel, R., M. Dreger, C. Gillen, O. Bender, J. Kurreck, and F. Hucho. 2001. Biochemical characterization of the vanilloid receptor 1 expressed in a dorsal root ganglia derived cell line. *Eur. J. Biochem.* 268:5489–5496.

Jin, X., J. Touhey, and R. Gaudet. 2006. Structure of the N-terminal ankyrin repeat domain of the TRPV2 ion channel. *J. Biol. Chem.* 281:25006–25010.

Johnson, J.P., Jr., and W.N. Zagotta. 2001. Rotational movement during cyclic nucleotide-gated channel opening. *Nature.* 412:917–921.

Jordt, S.E., D.D. McKemy, and D. Julius. 2003. Lessons from peppers and peppermint: the molecular logic of thermosensation. *Curr. Opin. Neurobiol.* 13:487–492.

Kedei, N., T. Szabo, J.D. Lile, J.J. Treanor, Z. Olah, M.J. Iadarola, and P.M. Blumberg. 2001. Analysis of the native quaternary structure of vanilloid receptor 1. *J. Biol. Chem.* 276:28613–28619.

Kitahara, T., H.S. Li, and C.D. Balaban. 2005. Changes in transient receptor potential cation channel superfamily V (TRPV) mRNA expression in the mouse inner ear ganglia after kanamycin challenge. *Hear. Res.* 201:132–144.

Kuzhikandathil, E.V., H. Wang, T. Szabo, N. Morozova, P.M. Blumberg, and G.S. Oxford. 2001. Functional analysis of capsaicin receptor (vanilloid receptor subtype 1) multimerization and agonist responsiveness using a dominant negative mutation. *J. Neurosci.* 21:8697–8706.

Lakowicz, J. 1999. Principles of Fluorescence Spectroscopy. Plenum Publishing Corp., New York. 725 pp.

Li, M., J. Jiang, and L. Yue. 2006. Functional characterization of homo- and heteromeric channel kinases TRPM6 and TRPM7. *J. Gen. Physiol.* 127:525–537.

Liapi, A., and J.N. Wood. 2005. Extensive co-localization and heteromultimer formation of the vanilloid receptor-like protein TRPV2 and the capsaicin receptor TRPV1 in the adult rat cerebral cortex. *Eur. J. Neurosci.* 22:825–834.

Lintschinger, B., M. Balzer-Geldsetzer, T. Baskaran, W.F. Graier, C. Romanin, M.X. Zhu, and K. Groschner. 2000. Coassembly of Trp1 and Trp3 proteins generates diacylglycerol- and Ca^{2+}-sensitive cation channels. *J. Biol. Chem.* 275:27799–27805.

Liu, X., B.C. Bandyopadhyay, B.B. Singh, K. Groschner, and I.S. Ambudkar. 2005. Molecular analysis of a store-operated and 2-acetyl-sn-glycerol-sensitive non-selective cation channel. Heteromeric assembly of TRPC1-TRPC3. *J. Biol. Chem.* 280:21600–21606.

McCleverty, C.J., E. Koesema, A. Patapoutian, S.A. Lesley, and A. Kreusch. 2006. Crystal structure of the human TRPV2 channel ankyrin repeat domain. *Protein Sci.* 15:2201–2206.

McKemy, D.D., W.M. Neuhausser, and D. Julius. 2002. Identification of a cold receptor reveals a general role for TRP channels in thermosensation. *Nature.* 416:52–58.

Minke, B., and B. Cook. 2002. TRP channel proteins and signal transduction. *Physiol. Rev.* 82:429–472.

Montell, C., L. Birnbaumer, and V. Flockerzi. 2002. The TRP channels, a remarkably functional family. *Cell.* 108:595–598.

Moran, M.M., H. Xu, and D.E. Clapham. 2004. TRP ion channels in the nervous system. *Curr. Opin. Neurobiol.* 14:362–369.

Patapoutian, A., A.M. Peier, G.M. Story, and V. Viswanath. 2003. ThermoTRP channels and beyond: mechanisms of temperature sensation. *Nat. Rev. Neurosci.* 4:529–539.

Peier, A.M., A.J. Reeve, D.A. Andersson, A. Moqrich, T.J. Earley, A.C. Hergarden, G.M. Story, S. Colley, J.B. Hogenesch, P. McIntyre, et al. 2002. A heat-sensitive TRP channel expressed in keratinocytes. *Science.* 296:2046–2049.

Poteser, M., A. Graziani, C. Rosker, P. Eder, I. Derler, H. Kahr, M.X. Zhu, C. Romanin, and K. Groschner. 2006. Trpc3 and trpc4

associate to form a redox-sensitive cation channel-evidence for expression of native trpc3/trpc4 heteromeric channels in endothelial cells. *J. Biol. Chem.* 281:13588–13595.

Qin, F., A. Auerbach, and F. Sachs. 2000. Hidden Markov modeling for single channel kinetics with filtering and correlated noise. *Biophys. J.* 79:1928–1944.

Rizzo, M.A., G.H. Springer, B. Granada, and D.W. Piston. 2004. An improved cyan fluorescent protein variant useful for FRET. *Nat. Biotechnol.* 22:445–449.

Rosenbaum, T., and S.E. Gordon. 2002. Dissecting intersubunit contacts in cyclic nucleotide-gated ion channels. *Neuron.* 33:703–713.

Rutter, A.R., Q.P. Ma, M. Leveridge, and T.P. Bonnert. 2005. Heteromerization and colocalization of TrpV1 and TrpV2 in mammalian cell lines and rat dorsal root ganglia. *Neuroreport.* 16:1735–1739.

Ryu, S., B. Liu, and F. Qin. 2003. Low pH potentiates both capsaicin binding and channel gating of VR1 receptors. *J. Gen. Physiol.* 122:45–61.

Schaefer, M. 2005. Homo- and heteromeric assembly of TRP channel subunits. *Pflugers Arch.* 451:35–42.

Selvin, P.R. 1995. Fluorescence resonance energy transfer. *In* Methods in Enzymology. Volume 246. Academic Press, Inc., Orlando, FL. 300–334.

Smith, G.D., M.J. Gunthorpe, R.E. Kelsell, P.D. Hayes, P. Reilly, P. Facer, J.E. Wright, J.C. Jerman, J.P. Walhin, L. Ooi, et al. 2002. TRPV3 is a temperature-sensitive vanilloid receptor-like protein. *Nature.* 418:186–190.

Strubing, C., G. Krapivinsky, L. Krapivinsky, and D.E. Clapham. 2001. TRPC1 and TRPC5 form a novel cation channel in mammalian brain. *Neuron.* 29:645–655.

Strubing, C., G. Krapivinsky, L. Krapivinsky, and D.E. Clapham. 2003. Formation of novel TRPC channels by complex subunit interactions in embryonic brain. *J. Biol. Chem.* 278:39014–39019.

Takanishi, C.L., E.A. Bykova, W. Cheng, and J. Zheng. 2006. GFP-based FRET analysis in live cells. *Brain Res.* 1091:132–139.

Tobin, D., D. Madsen, A. Kahn-Kirby, E. Peckol, G. Moulder, R. Barstead, A. Maricq, and C. Bargmann. 2002. Combinatorial expression of TRPV channel proteins defines their sensory functions and subcellular localization in *C. elegans* neurons. *Neuron.* 35:307–318.

Tsien, R.Y. 1998. The green fluorescent protein. *Annu. Rev. Biochem.* 67:509–544.

Venkataramanan, L., and F.J. Sigworth. 2002. Applying hidden Markov models to the analysis of single ion channel activity. *Biophys. J.* 82:1930–1942.

Voets, T., K. Talavera, G. Owsianik, and B. Nilius. 2005. Sensing with TRP channels. *Nat. Chem. Biol.* 1:85–92.

Vos, M.H., T.R. Neelands, H.A. McDonald, W. Choi, P.E. Kroeger, P.S. Puttfarcken, C.R. Faltynek, R.B. Moreland, and P. Han. 2006. TRPV1b overexpression negatively regulates TRPV1 responsiveness to capsaicin, heat and low pH in HEK293 cells. *J. Neurochem.* 99:1088–1102.

Vriens, J., A. Janssens, J. Prenen, B. Nilius, and R. Wondergem. 2004. TRPV channels and modulation by hepatocyte growth factor/scatter factor in human hepatoblastoma (HepG2) cells. *Cell Calcium.* 36:19–28.

Watanabe, H., J. Vriens, S.H. Suh, C.D. Benham, G. Droogmans, and B. Nilius. 2002. Heat-evoked activation of TRPV4 channels in a HEK293 cell expression system and in native mouse aorta endothelial cells. *J. Biol. Chem.* 277:47044–47051.

Xu, H., I.S. Ramsey, S.A. Kotecha, M.M. Moran, J.A. Chong, D. Lawson, P. Ge, J. Lilly, I. Silos-Santiago, Y. Xie, et al. 2002. TRPV3 is a calcium-permeable temperature-sensitive cation channel. *Nature.* 418:181–186.

Xu, X.Z., F. Chien, A. Butler, L. Salkoff, and C. Montell. 2000. TRPγ, a *Drosophila* TRP-related subunit, forms a regulated cation channel with TRPL. *Neuron.* 26:647–657.

Xu, X.Z., H.S. Li, W.B. Guggino, and C. Montell. 1997. Coassembly of TRP and TRPL produces a distinct store-operated conductance. *Cell.* 89:1155–1164.

Zagotta, W.N., N.B. Olivier, K.D. Black, E.C. Young, R. Olson, and E. Gouaux. 2003. Structural basis for modulation and agonist specificity of HCN pacemaker channels. *Nature.* 425:200–205.

Zhang, L., S. Jones, K. Brody, M. Costa, and S.J. Brookes. 2004. Thermosensitive transient receptor potential channels in vagal afferent neurons of the mouse. *Am. J. Physiol. Gastrointest. Liver Physiol.* 286:G983–G991.

Zheng, J. 2006. Spectroscopy-based quantitative fluorescence resonance energy transfer analysis. *Methods Mol. Biol.* 337:65–78.

Zheng, J., and F.J. Sigworth. 1998. Intermediate conductances during deactivation of heteromultimeric *Shaker* potassium channels. *J. Gen. Physiol.* 112:457–474.

Zheng, J., M.C. Trudeau, and W.N. Zagotta. 2002. Rod cyclic nucleotide-gated channels have a stoichiometry of three CNGA1 subunits and one CNGB1 subunit. *Neuron.* 36:891–896.

Zheng, J., L. Vankataramanan, and F.J. Sigworth. 2001. Hidden Markov model analysis of intermediate gating steps associated with the pore gate of shaker potassium channels. *J. Gen. Physiol.* 118:547–564.